Origins of correlated spiking in the mammalian olfactory bulb

Richard C. Gerkin[a,b,c,1], **Shreejoy J. Tripathy**[b], **and Nathaniel N. Urban**[a,b,1]

[a]Department of Biological Sciences and [b]Center for the Neural Basis of Cognition, Carnegie Mellon University, Pittsburgh, PA 15213; and [c]School of Life Sciences, Arizona State University, Tempe, AZ 85287

Edited by Charles F. Stevens, The Salk Institute for Biological Studies, La Jolla, CA, and approved September 5, 2013 (received for review February 28, 2013)

Mitral/tufted (M/T) cells of the main olfactory bulb transmit odorant information to higher brain structures. The relative timing of action potentials across M/T cells has been proposed to encode this information and to be critical for the activation of downstream neurons. Using ensemble recordings from the mouse olfactory bulb in vivo, we measured how correlations between cells are shaped by stimulus (odor) identity, common respiratory drive, and other cells' activity. The shared respiration cycle is the largest source of correlated firing, but even after accounting for all observable factors a residual positive noise correlation was observed. Noise correlation was maximal on a ∼100-ms timescale and was seen only in cells separated by <200 μm. This correlation is explained primarily by common activity in groups of nearby cells. Thus, M/T-cell correlation principally reflects respiratory modulation and sparse, local network connectivity, with odor identity accounting for a minor component.

olfaction | synchrony | sensory | statistics

Mitral/tufted cells (M/Ts) of the olfactory bulb (OB) receive odor-evoked activity from sensory neurons and transmit it to central brain structures. Thus, understanding how odor information is represented by these neurons' activity is essential to understanding olfactory coding. Studying coding properties at this stage in the olfactory system is particularly interesting because the small number of M/Ts (∼50,000) compared with sensory neurons (∼10 million) or olfactory cortical neurons (∼2 million) suggests that this stage represents a bottleneck (1).

Odor information is encoded in the spatial pattern of activity across the OB (2). However, the timing of M/T activity may also play a crucial role in odor representation. Individual M/Ts fire odor-specific patterns of spikes (3), and spike timing across populations of M/Ts relative to the respiration cycle has been proposed as an olfactory code (4, 5). However, whether odor identity influences the correlation of M/T activity (i.e., the tendency of neurons to spike together) has not been specifically addressed.

Ensemble firing patterns better predict odorant identity than do single neuron firing rates alone (6, 7), suggesting the utility of a population timing code. Additionally, learned olfactory behaviors are associated with increased M/T spike synchrony (8), and disrupting this synchrony in insect M/T analogs reduces odor discriminability (9). Furthermore, analysis of neural correlations has informed our understanding of the relationship between neural circuits and population activity and has constrained hypotheses concerning "decoding" of incoming population activity by downstream areas (10).

Here, we evaluated how relative M/T timing depends upon odor identity and timing, respiration phase (inhalation/exhalation), and other neurons' spiking. Correlated spiking in the OB is familiar (11, 12), but how these correlations depend on such variables is unknown. Correlations may originate in common stimulus or respiration phase preferences ("signal correlation"). Cell pairs' spiking may also exhibit covariation beyond that predicted from such preferences ("noise correlation," R_{noise}) and may reflect correlated input noise or synaptic coupling between cells (13, 14). In *Xenopus* and *Drosophila*, M/Ts and their analogs exhibit significant noise correlation (15, 16). However, the origins, magnitude, and scope of such correlations have not been described in the mammalian OB.

Critically, correlation driven by respiration or population activity in the local circuit has not been estimated, yet this is required to understand the sources and possible functions of OB correlations, and the theoretical coding capacity and mechanisms of OB neural ensembles (17, 18). We contrast our analysis to the computation of trial-averaged population response correlations (i.e., "pattern correlations"). Our approach is more analogous to that of, for example, Kazama and Wilson (16): We address within-trial spike-timing correlations between cell pairs rather than correlations between trial-averaged responses to different odorants (19).

We made ensemble recordings from mouse OB during odor presentation. From these recordings we isolated contributions of several olfactory variables to spiking in individual neurons and to intercell correlation. Respiration phase tuning accounts for much correlation, whereas some nearby cell pairs exhibit small, positive R_{noise}, independent of the stimulus. Conditional on the activity of the larger population, functional coupling between cells is sparse overall, with significant implications for olfactory coding.

Results

Tetrodes were placed in the OB of anesthetized mice ($n = 4$ mice) to record M/T spiking. Single-unit activity was detected on each tetrode in the mitral cell layer, and several dozen units (37–64) were isolated for further analysis. The respiration cycle, which lasted 300–500 ms (2–3 Hz), was characterized by clear epochs of inhalation and exhalation (Fig. 1 *A* and *B*). The firing rates of M/Ts strongly covary with the phase of this cycle (20). Our data showed that most cells (63.2%) exhibited at least two-thirds of their spikes in half of the cycle, with most firing maximally just after the boundary between the end of inspiration and the onset of expiration (Fig. 1*C* and Fig. S1). Modulation by respiration was usually stronger than modulation by odor (Fig. 1*D*).

Significance

Neurons exhibit temporally correlated patterns of activity, and the brain is believed to process information in part by exploiting these correlations. Here we use new analytic tools to show that in the olfactory bulb, the first processing station for smell in mammals, these correlations emerge primarily from the animal's own breathing pattern, and also from the sparse connectivity of the cells that ultimately transmit olfactory information to higher brain areas. These results inform our understanding of how, and how well, the brain can represent information about smell and provide insight into the importance of active sampling processes in sensory coding.

Author contributions: R.C.G., S.J.T., and N.N.U. designed research; R.C.G. performed research; R.C.G. contributed new reagents/analytic tools; R.C.G. analyzed data; and R.C.G., S.J.T., and N.N.U. wrote the paper.

The authors declare no conflict of interest.

This article is a PNAS Direct Submission.

[1]To whom correspondence may be addressed. E-mail: rgerkin@asu.edu or nurban@cmu.edu.

This article contains supporting information online at www.pnas.org/lookup/suppl/doi:10.1073/pnas.1303830110/-/DCSupplemental.

NEUROSCIENCE

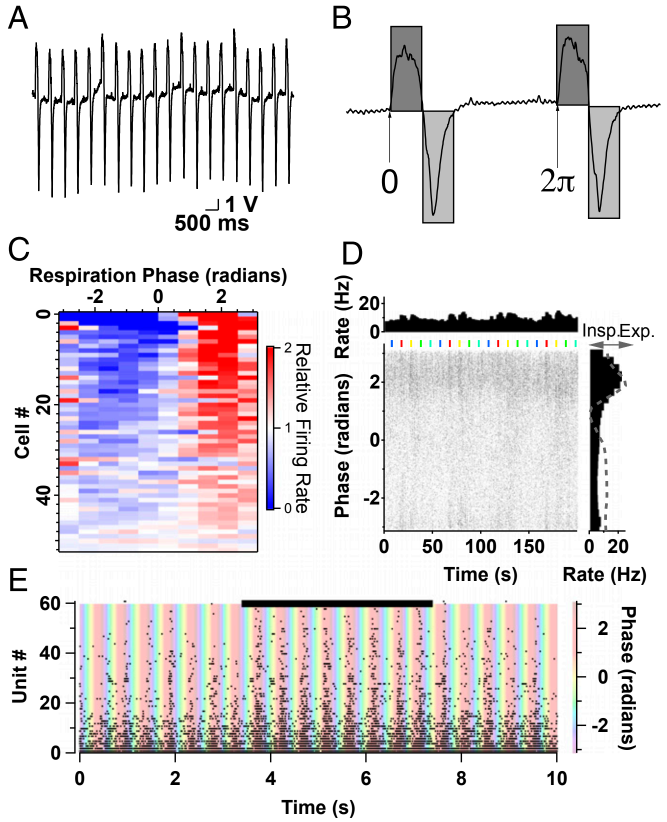

Fig. 1. Respiration drives changes in M/T cell firing rates. (*A*) Filtered (1–30 Hz) recording of respiration via a piezoelectric chest cuff. (*B*) Two representative respiration cycles, with inspiration (dark rectangle) and expiration (light rectangle) noted. Phase convention is indicated; 0 is the onset of inspiration. Actual phase estimates are computed via wavelet transform and shifted to match this convention. (*C*) Cyclohistograms from one set of simultaneously recorded neurons, sorted by tuning index, indicating the firing rate relative to that expected for uniform spiking across the respiration cycle. (*D*) Comparison of firing modulation by phase and by odor for an example neuron during 200 s of recording. The depth of modulation by respiration phase (right) exceeds that by presentation of odor (top, duration of each of five odors indicated by a corresponding colored bar). (*E*) Comparison of modulation for many simultaneously recorded neurons during one 10-s trial. Neurons are ordered by firing rate. Presentation of an acetate mixture is indicated by the black bar, and respiration phase is indicated by the colored background.

Spiking of M/T Cell Pairs Is Correlated. We asked whether information about odor identity is encoded in the temporal structure of spiking in neuronal populations, as suggested previously (7, 8). We measured spiking responses of M/T ensembles to odor stimulus (Fig. S2) and computed the correlation structure of cells' responses (*Methods* and Fig. S3 *A* and *B*). Prominent low-frequency peaks due to respiration coupling were typically observed, i.e., cells consistently fired at the same relative phases of the respiration cycle. Because correlations on different timescales arise from different mechanisms and have different implications for stimulus encoding (21), we computed spike-count correlation coefficients ("correlation") for M/T pairs using various bin sizes. Correlation was largest at bin sizes of 200–500 ms (Fig. S3*C*).

Nonzero correlation in spiking of two cells can arise from shared synaptic input, direct coupling, or other factors such as odor tuning, respiration tuning, intratrial response kinetics, and trial position during the experiment (i.e., accounting for slow trial-to-trial drift). We used several different methods to estimate the fraction of correlation accounted for by each factor and, conversely, how much correlation remained unexplained.

Noise Correlation and Coherence in M/T Cell Pairs. Noise correlation is usually computed by first subtracting the mean response to a "signal" before computing within-trial correlation between cells. We generalized this approach to place any subset of factors, not just the stimulus, into the category of signal (*Methods* and *Supporting Information*). Thus, R_{noise} can be computed according to a "noise" definition that includes any or even all measured factors, and thus reflects truly unexplained or surprising correlated firing.

We computed correlation following the identification of specific factors with "signal" or "noise." This revealed correlation due to common odor tuning, common respiration phase tuning, and slow (tens of seconds) changes in population firing rates across trials (Fig. S4). The residual correlation when all measured covariates are treated as "signal" is the most stringent estimate of noise correlation (i.e., it provides the smallest upper bound, reflecting the correlation not explained by the available measurements). We computed R_{noise} in a variety of bin sizes and found a peak at 100 ms (Fig. 2*A*, $n = 4$ mice). At this timescale, we generated the R_{noise} matrix for cell pairs (Fig. 2*B*, representative experiment). This matrix was considerably sparser than the raw correlation matrix, because most correlations are explained by the signal. To test whether correlation depended on potential glomerular association of M/T cell pairs, we compared cells recorded on the same tetrode (NEAR) and those recorded on different tetrodes (FAR). Interestingly, very few FAR pairs (5.8%, n = 7,842 pairs, four mice) had R_{noise} values differing significantly ($P < 0.001$) from zero, whereas for NEAR pairs R_{noise} was frequently significantly greater than zero (54.5%, n = 2,172 pairs, four mice) (Fig. 2 *C* and *D*). These estimates were not due to spurious correlations generated by spike-sorting artifacts (Fig. S5).

We next analyzed correlated spiking between cells in the frequency domain, where the effects of periodic forces such as respiration or other intrinsic rhythms would be clearly manifest. Rather than conditioning on sets of factors as above, we calculated spectral coherence using the raw spike trains (Fig. 2*E*). We observed that FAR cells exhibited coherence only at the respiration frequency, whereas NEAR cells exhibited broadband coherence (0.3–20 Hz, Fig. 2*F*, four mice). This indicates that firing patterns of FAR cells are only related through their shared drive from respiration, whereas NEAR cell firing patterns are strongly correlated at a wide range of timescales.

Unlike correlation, its unnormalized form—covariance—is additive (*Methods*); thus, we can represent sources of covariance as parts of the total covariance (Fig. 2*G*). M/Ts fluctuate about their mean firing rates, and even when they do so together (i.e., they covary), it is only partly explained by observable factors. Under all conditions, noise covariance makes a major contribution to total covariance. In NEAR pairs, the unexplained component—the noise covariance—is 3.6 times greater than in FAR pairs, consistent with correlating circuit mechanisms in the NEAR pairs. Surprisingly, covariance driven by odor tuning is small and on average not significantly different from zero ($P > 0.3$), possibly reflecting that similarly and differently tuned pairs of cells contribute positive and negative odor covariance, respectively. Consistent with this interpretation, increasing the odor concentration fivefold increased the fraction of cells showing pure increases in firing rate (Fig. S2), and consequently increased odor covariance. This increase may also have been due to threshold firing rate effects (22). Covariance due to respiration tuning also increased with odor concentration, as spikes became more concentrated in each cell's preferred respiration phase.

Noise Correlation Is Invariant to the Stimulus. Finally, we tested whether odor alters noise correlation, beyond the effects it has on individual firing rates, as has been observed in primate visual and motor cortices (23). However, the rates of unexpected coincident spiking did not significantly differ in the odor-evoked and spontaneous period ($P > 0.15$, Kolmogorov–Smirnov test, Fig. S6). Consequently, odor did not seem to have any effect on

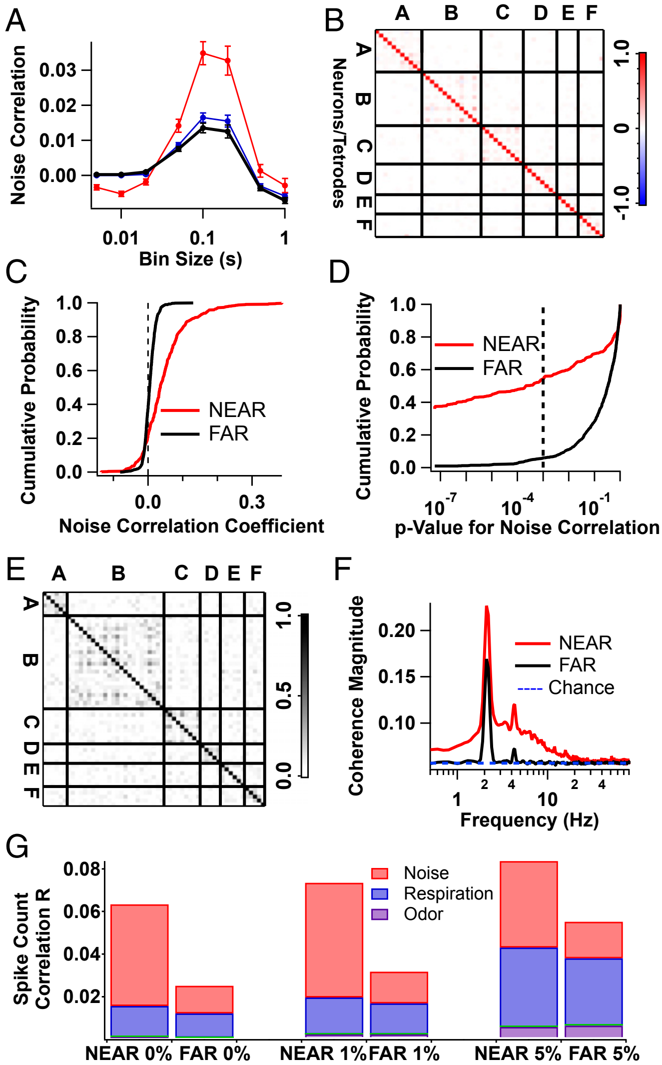

Fig. 2. Noise correlation is distance-dependent. (*A*) The mean R_{noise} between M/T cells peaks at a ~100-ms timescale. Pairs of cells recorded on the same tetrode (NEAR) are summarized in red; pairs on different tetrodes (FAR) are in black; average across all neurons is in blue. (*B*) R_{noise} matrix from one experiment. Each entry is one cell pair, and dark grid lines separate tetrodes. Nonzero R_{noise} is concentrated among NEAR cells (i.e., in on-diagonal boxes). (*C*) Cumulative histogram of R_{noise} shown in *B*. (*D*) *P* values (for the null hypothesis of $R_{noise} = 0$) for the data in *B*, obtained by shuffling. Vertical dashed line indicates $P = 0.001$. Note that ~50% of NEAR cell pairs have signficant R_{noise} at $P < 0.001$. (*E*) For a different experiment, a coherence matrix for recorded pairs, showing the median coherence in the 1- to 10-Hz range. (*F*) Coherence magnitude as a function of frequency. NEAR cells are coherent at a range of frequencies, whereas FAR cells only show coherence greater than chance at the respiration frequency and its harmonics. (*G*) Fraction of covariance explained by each source, represented by the relative height of each segment, and the total height of each bar equal to the mean spike count correlation for cell pairs. Three odor conditions are shown: spontaneous (no odor), 1% dilution, and 5% dilution.

noise correlation, nor did respiration phase preferences have any impact on the noise correlation between cell pairs (Fig. S5*E*).

Sparse Functional Coupling in M/T Cell Networks. The observed R_{noise} for NEAR pairs may reflect (1) unique firing patterns shared only by the pair itself (owing to, e.g., a synapse or gap junction between the pair), or they may be generated by (2) a broad pattern of similar activity observed across many cells, shared owing to circuit mechanisms (e.g., shared presynaptic inhibition).

We thus asked whether correlation observed in each cell pair was explained by the remaining cells' activity. We fit firing rates to a generalized linear model (GLM) (24, 25) containing the factors of interest, such as odor, respiration phase, and trial timing information (*Methods*). Specifically, the model yields the expected number of spikes emitted by a given cell in each time bin (Fig. 3*A*). Fitted model coefficients (which maximize the likelihood of the observed spiking data) can be used to assess and isolate the dependence of spiking on single factors (e.g., respiration, Fig. 3*B*). We compared models containing different explanatory factors, quantifying model predictive power through receiver-operating characteristic (ROC) analysis (Fig. 3*C*). Specifically, we asked how effective models using progressively larger subsets of factors were in predicting whether a neuron would spike in a given time bin (Fig. S7 and *Methods*).

We used this technique to determine which cell pairs were conditionally dependent under each model. Considering only cells' spike counts and slow stimulus-independent firing rate changes during the experiment, 63.7% of cell pairs were conditionally dependent (*Methods*). Additionally considering the identity and time course of odor stimulus reduced this only to 62.3% (Fig. 4*A*), indicating that odor stimulus accounted for very little correlated activity. Respiration strongly drives individual M/T cell activity, and accounting for respiration phase instead of odor left only 53.5% of pairs dependent (Fig. 4*B*). Accounting for odor and respiration phase reduced this to 48.0% (Fig. 4*C*). In other words, a majority of neuron pairs were conditionally independent when odor and respiration were both taken into account.

If large groups of cells have strongly covarying firing rates, owing to unmeasured stimulus fluctuations or to unobserved changes in internal brain state, then the population mean firing rate of the remaining cells might explain many cell-pair associations. Indeed, adding instantaneous population firing rate to the model left only 10.1% of cells conditionally dependent (Fig. 4*D*). This indicates that network-wide correlations—beyond those owing to

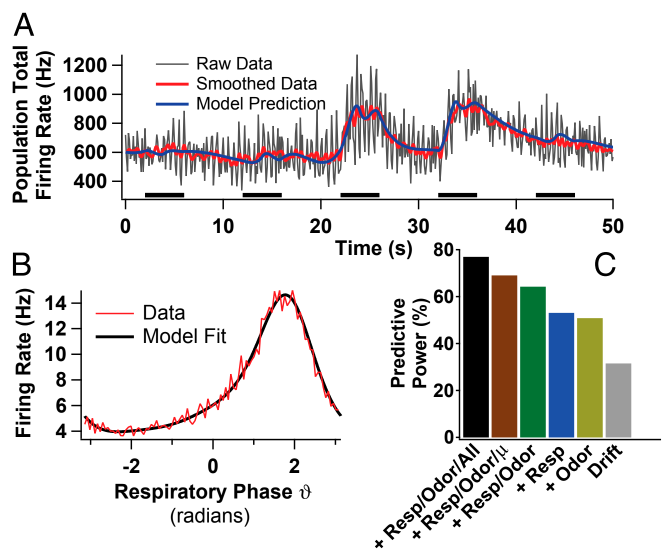

Fig. 3. A GLM for prediction of spiking. (*A*) Raw firing rate over five trials (five different odors) is shown in gray, a smoothing of that data in red, and a model prediction of the same responses in blue. The data in gray were not used to train the model (i.e., the prediction was out-of-sample). (*B*) The respiration phase preference (cyclohistogram) of an individual cell is well fit by the model, indicating that the modulation of firing by respiration has been well captured. (*C*) Predictive power of various candidate models, computed from ROC analyses. μ refers to the mean over all other recorded cells. "All" refers to all cells used individually as predictors.

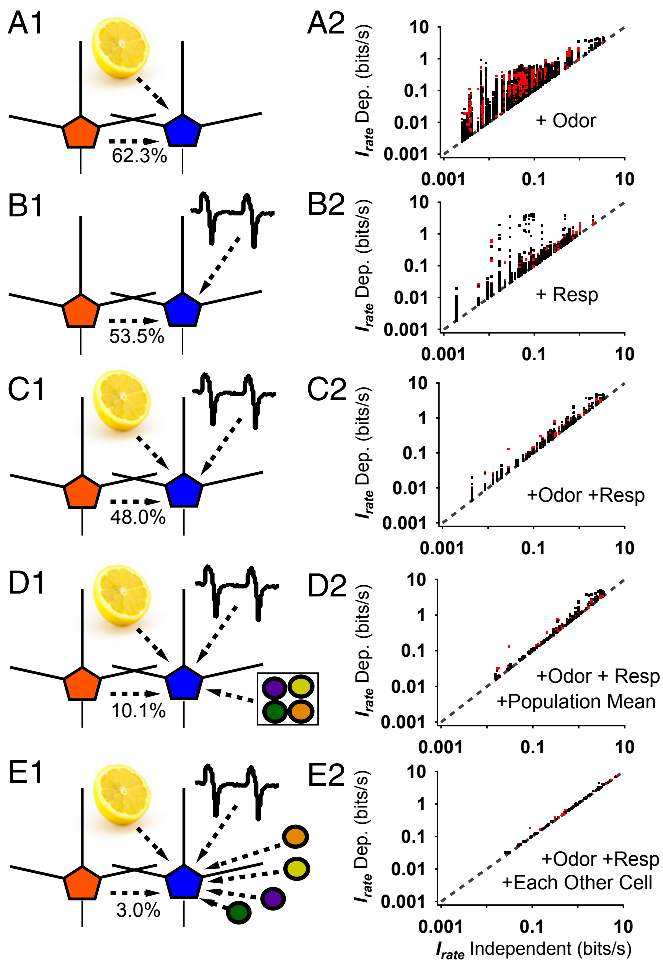

Fig. 4. Sparse functional connectivity in the M/T cell network. (*A1*) Schematic of two M/T cells, indicating a model in which odor identity and time course, plus spiking of the orange cell, are the only factors used to predict spiking in the blue cell. The fraction of cell pairs in which such a potential functional connection (orange to blue) is indicated by the spiking data is shown below the dashed arrow. (*B1*) Same as *A1* but with respiration phase as a predictor instead of odor. Fewer other cells (orange) are useful in predicting the spiking of a given cell (blue) when respiration phase is known, so the functional connectivity decreases (i.e., more cell pairs are conditionally independent given respiration than given odor). (*C1*) Similar to *A1* and *B1*, but with both respiration and odor as predictors. (*D1*) Same as *C1*, but including population mean firing rate. (*E1*) Same as *C1*, but including the instantaneous firing rate of each other simultaneously recorded cell. In this final case, functional connectivity is only indicated if two cells' spike patterns are conditionally dependent when conditioned upon all other observable data recorded in an experiment. (*A2*–*E2*) Comparison of information gain (compared with a naive mean firing rate model) for the dependent model (i.e., including the orange-to-blue associations) vs. the independent model (does not include the orange-to-blue associations). Points falling on the diagonal line indicate cell pairs that were conditionally independent given the other model factors. Red and black dots represent NEAR and FAR cell pairs, respectively.

respiration or odor, and summarized only by the population mean firing rate—explained much of these neurons' activity.

If functional connections (i.e., statistical dependencies) between cell pairs are rare, then a cell ensemble is described as sparsely coupled. We fit a complete model for each cell in which the individual spiking pattern of each other cell was a separate factor. This model, containing disaggregated information about firing patterns of dozens of other neurons, was more predictive than the model using population mean firing rates (Fig. 3*C*). Indeed, in this analysis only 3.0% of pairs of cells remained conditionally dependent (Fig. 4*E*). In other words, given knowledge of respiration and odor context, and a large number of other cells' spike patterns, further knowing the spiking pattern of cell *Y* only helps to predict spiking in cell *X* in 3% of cell pairs.

Discussion

Mammalian M/T cell pairs in vivo exhibit correlated spiking at timescales of tens to hundreds of milliseconds. We analyzed the sources of this correlation and show that it is driven largely by similarity in preferred respiration phase, but that controlling for this factor leaves significant noise correlation (R_{noise}). R_{noise} (and broad-band coherence) is negligible for cells recorded on tetrodes separated by ≥150 μm (FAR) but significantly positive for approximately half of cell pairs recorded on the same tetrode (NEAR). NEAR correlation is largely but not totally explained by the covariation of each cell's spiking with the population response, rather than by pairwise relationships between specific cells. However, the sparse functional coupling we observe should not be interpreted as a paucity of anatomical coupling, just as, conversely, a small probability of pairwise synaptic connectivity is sufficient to generate correlation in all cell pairs (26). Nonetheless, it implies that very few M/T cell pairs have patterns of activity associated in time as strongly as one might predict under direct anatomical coupling.

Local Circuits Mediating NEAR Noise Correlation. What circuits underlie noise correlation in NEAR cell pairs? Anatomical analysis indicates that cells >200 μm apart are unlikely to be sister cells (receiving input from the same glomerulus) (27–29). Together with our electrode configuration, this implies that FAR cells are unlikely to be sisters, and that most sister cells in our dataset are NEAR cells (*Supporting Information* and Fig. S8).

Whereas receiving input from the same glomerulus would certainly explain signal correlation in M/T cell pairs, nonzero R_{noise} owing to shared sensory input would require shared input noise on the timescale where R_{noise} is maximal (∼100 ms, Fig. 2*A*), and possibly other timescales (Fig. 2*F*). Synaptic depression may provide such a mechanism (16), or NEAR M/T cell pairs may share lateral intraglomerular circuitry, perhaps from shared stochastic inhibition from common periglomerular cells. Analogous circuitry requirements have been suggested in visual cortex to explain the distance dependence of R_{noise} (21). Raw cross-correlation is elevated in NEAR cells in other olfactory preparations (16, 30, 31), and noise correlation in sister cells has been measured in nonmammalian olfactory structures (15, 16). Alternatively, finite dendritic length in granule cells, which limits the range of connectivity (32), may also introduce spatially dependent correlations. Barrages of inhibitory postsynaptic currents from granule cells can last ∼100 ms, owing in part to the temporally distributed activity of granule cells (33). If these barrages are correlated across sister M/Ts, they could generate R_{noise} on the timescale observed here (34). Indeed, nearby cells show higher-order and stronger correlations than distant cells in cortical circuits (21, 35).

Nonzero correlation for NEAR pairs is not an artifact of spike sorting (Fig. S5). In cases in which R_{noise} is zero (36), as in FAR pairs here, proposed mechanisms are (*i*) lack of input correlation or (*ii*) active decorrelation by circuits (14, 37). These could be distinguished by measuring subthreshold responses from sister and nonsister M/T cell pairs in vivo.

Stimulus Dependence of Correlation. We found no evidence for a dependence of R_{noise} on the presence or timing of the odor stimulus. In part, this indicates that we have effectively separated signal and noise sources of correlation; indeed, raw correlation of M/T cell pairs typically rises upon odor presentation—but only to the degree expected from shared odor tuning preferences. Stimulus dependence of noise correlation has been observed in the visual system (21, but see ref. 38), although it is generated by special circuitry that the OB is unlikely to share. In the fly olfactory system (16), odor markedly increases noise correlation.

Because flies have just two sister projection neurons (M/T cell analogs) vs. dozens of sister M/T cells in a rodent glomerulus, stimulus-dependent increases in R_{noise} might be less important in the rodent olfactory system for coordinating a suprathreshold postsynaptic response in downstream targets, because there would already be sufficient drive from a larger population of inputs. One major downstream target of the mammalian OB is the anterior piriform cortex, where millions of neurons receive divergent output from the OB and noise correlation is low (39) and quenched completely by the stimulus (39). The further from the sensory periphery, the more important spike count and the less important spike timing within sampling "frames" (e.g., respiration cycles) may be (39); nonetheless, understanding the olfactory system precisely will require quantitative modeling of spiking activity at the appropriate timescale.

State-Dependent Sources of Correlation. Our experiments were performed under sevoflurane anesthetic, generating lower firing rates (40) and sparser glomerular activation (41) than in awake recordings (Table S1). However, M/T cell odor-evoked responses are similarly sparse under both sevoflurane-anesthetized and awake animals (40), and more sparse than under ketamine anesthesia (42). Patterns of direct glomerular activation in awake mice are similar to those under ketamine, but diverge at the infraglomerular level, possibly owing to state-dependent differences in activity along M/T cell lateral dendrites (43) or in effective coupling strength. Indeed, the strength of lateral inhibition depends nonlinearly on the firing rate of postsynaptic targets (44) and thus may vary across brain states with different firing rates.

Recordings in awake animals are also likely to be influenced by other endogenous sources of correlation, such as variable levels of arousal, resulting in increased apparent noise correlation; these variables may be behaviorally relevant (14, 45) but challenging to estimate (36). This increased variability in the awake state may be largely due to variability in the awake respiration pattern, because accounting for temporal dynamics in the bulb as a whole substantially reduces response variability across sniffs (43). This suggests that the techniques described here will be readily applicable to the study of awake, behaving mice.

Estimation of Noise Correlation in the OB. Estimating R_{noise} requires identifying and controlling for experimental variables [such as the stimulus or slow firing rate drift (38)] that cause covariation of responses. Systems using active sampling or in which slow fluctuations generate correlations across many cells pose a special challenge; active sampling will generate covariation of activity that may be uncorrelated with stimulus delivery. Computing R_{noise} in systems using active sampling such as the mammalian OB requires an additional technical innovation: accounting for the effect of a driving signal on observed correlation. This innovation, developed and applied here (*Methods* and *Supporting Information*) will be of general use when trying to control for the contribution of signals that may drive spiking and, by extension, correlation.

The effects of correlation on coding can be complex (34). Correlated spiking can help transmit a signal to postsynaptic targets via temporal summation of synaptic potentials. Even if correlation is unrelated to the stimulus, for example, R_{noise}, this mechanism may preferentially propagate signals coming from the most active cells (e.g., those responding to the stimulus) and thus aid the transmission of useful information. Intuitively, however, knowing whether a firing rate change is due to signal or noise is useful and is a valuable component of neural coding (10). For example, noise correlation can compromise information transmission by reducing the effective number of independent signal estimates (17). That is, when noise is correlated, it does not "average out" when pooling neurons. Even at the levels of R_{noise} reported here, information would begin to saturate in pools of as few as 25 neurons (17) (*Supporting Information*), comparable to the ~25 M/T cells receiving input from a single glomerulus in the rodent OB (46), and far lower than the estimated 50,000 M/T cells across all glomeruli (46). An intriguing possibility is that levels of noise correlation are matched to population sizes, and larger populations (as in vertebrate sister M/T cells) require smaller values of R_{noise} than smaller populations (as in invertebrate sister projection neurons) to make use of numerical advantage for information transmission. However, when stimulus preferences are heterogeneous, the optimal R_{noise}—maximizing information content—is greater than zero (18). Indeed, M/T cells have heterogeneous response properties, owing in part to variable biophysical properties (47). Thus, nonzero noise correlation may be preferable by virtue of enabling more odor information to be faithfully transmitted.

Methods

Electrophysiology. Signals were amplified and filtered between 600–6,000 Hz and visualized and recorded using Cheetah software (Neuralynx). Units were sorted offline using Klustawik (http://klustawik.sourgeforge.net). Units with an isolation distance >25 were considered to have good isolation (48); an example tetrode is shown in Fig. S5. There was no dependence (r = 0.07) of R_{noise} for NEAR pairs on their pairwise L ratio (48), ruling out spike-sorting artifacts for the NEAR cell pair results (14, 49). Data presented here are taken from the single ensemble of simultaneously recorded neurons in each animal (six to eight tetrodes per recording) yielding the largest number of high-quality single units. Total data used here are n = 4 animals and n = 177 single units.

Odor Delivery. In each experiment mice were presented with a series of four odor mixtures [odors A, B,E, and F from figure 2 of Bozza et al. (50), corresponding to alcohols, carboxylic acids, acetates, and ketones], each with eight mixture components present at 1–5% (8–40% total) in light mineral oil. Mixtures were chosen to increase single M/T cell responses (40) and because ethological relevant odorants are rarely unimolecular. A fifth "blank" mixture contained only light mineral oil and served as a control; a pure odorant (10% isoamyl acetate) was also used for comparison.

Data Analysis. Respiration phase was computed using a continuous wavelet transform of the respiration signal, assessed at the respiration frequency, which varied across experiments between 2–3 Hz. This yielded a consistent phase estimate lacking discontinuities. Each cycle phase increased linearly in time from 0 to 2π, and cyclohistograms were computed using 10 equally spaced bins within each cycle. The respiration tuning index was computed as $(f_{max} - f_{min})/(f_{max} + f_{min})$, with f_{max} and f_{min} the firing rates at preferred and antipreferred respiration phases, respectively.

Correlation matrices come from single recordings, whereas summary histograms are averages across recordings. Cross-correlation functions were calculated with no corrections in 10-ms bins and use the Pearson correlation R of cells' spike count time series for a range of lags Δt. R as a function of bin size (Fig. S3 *C* and *D*) is calculated at $\Delta t = 0$. R_{noise} was computed according to the law of total covariance:

$$\mathrm{cov}(X,Y) = E[\mathrm{cov}(X,Y|Z)] + \mathrm{cov}(E[X|Z],E[Y,Z]), \quad [1]$$

where cov denotes covariance and E[X] denotes the expectation value of X. The total covariance cov(X,Y) is the spike count covariance for cells X and Y (i.e., the covariance of spike count vectors for the entire recording session). The noise covariance, cov(X,Y|Z), represents the spike count covariance conditional upon a factor Z, which represents known or "signal" experimental factors such as clock time, odor, and respiration phase. E[X|Z] is the expectation of cell X's spike count when these experimental factors take the value Z. This is estimated from data. For instance, if Z contains only odor identities (or only respiration phases) then E[X|Z] is an odor tuning curve (or a cyclohistogram). When Z contains multiple signals $Z_1,\ldots,Z_n$, we assume, consistent with a model in which covariates influence spike rates additively, that covariance adds linearly:

$$\mathrm{cov}(E[X|Z],E[Y,Z]) = \mathrm{cov}(E[X|Z_1],E[Y,Z_1]) + \ldots + \mathrm{cov}(E[X|Z_n],E[Y,Z_n]). \quad [2]$$

Once Eq. **1** has been solved for E[cov(X,Y|Z)], an analogous procedure is applied to obtain E[var(X|Z)] and E[var(Y|Z)] and we compute R_{noise} as

$$R_{noise} = E[\mathrm{cov}(X,Y|Z))/\mathrm{sqrt}(\mathrm{var}(X|Z)) * (\mathrm{var}(Y|Z))]. \quad [3]$$

In summary, R_{noise} is obtained by subtracting covariances of conditional spike counts from total covariance and normalizing. This goes beyond the classical

R_{noise} calculation that considers only one time series, the stimulus time course (13). A full derivation and justifications for assumptions are given in *Supporting Information*. The fraction of cell pairs exhibiting significant correlation was assessed using the false discovery rate (FDR) method (51), accounting for multiple comparisons.

Generalized Linear Model. The spike count model took the form

$$\ln(\mu_t) = \beta_{0t} + \beta_1 x_{1t} + \beta_2 x_{2t} + \ldots, \quad [4]$$

where μ_t is the mean expected spike count in bin t, each x_{it} is an observation of covariate (i.e., factor) i in bin t, and each β_i is a coefficient obtained from fitting to data. Thus, linear combinations of covariates x_{it}, each of which are observed values or simple transformations thereof, yield a predicted log firing rate. This class of model is a generalization of linear regression, except with a logarithmic (instead of a linear) relationship between spike count and its predictors, and a Poisson (instead of Gaussian) assumption about remaining uncertainty (24, 25). The full model is described in *Supporting Information*, but a key feature is the use of an exponentiated Fourier basis for respiration, $\Sigma_m[a_m \sin(m\theta_t) + b_m \cos(m\theta_t)]$ for $m = 1,2,3$, where θ_t is the respiration phase in bin t, and exponentiation implied by the logarithm in Eq. **4**. Substitution of the identity $\cos(\theta - \theta_0) = \cos(\theta)\cos(\theta_0) - \sin(\theta)\sin(\theta_0)$ yields a higher-order generalization of the von Mises distribution for the respiration phase of spikes, which agrees remarkably well with the empirical spike phase distribution (Fig. 3*B*)—this feature of the model is what enables the contribution of respiration to spiking to be cleanly separated from the contributions of other covariates.

Significant coupling of a cell Y to a reference cell X was assessed by fitting the model for X both with and without a term for spiking of Y, computing the deviance and comparing to a χ^2 distribution with one degree of freedom to obtain a P value. Cells exhibiting significant coupling to X were those with $P < \alpha$ (typically 0.01), that is, those significantly improving prediction of X's spike counts, subject to the FDR method for multiple comparisons correction. Results for other values of α are shown in Fig. S9.

ROC curves were constructed by fitting an alternative GLM, using a binary response variable (at least one spike vs. no spikes) and follow the method of Trucculo et al. (25), elaborated in Fig. S7. This took the form

$$\ln(p_t/(1-p_t)) = \beta_0 + \beta_1 x_1 + \beta_2 x_2 + \ldots \quad [5]$$

and was used because the concepts of "hits" and "misses" require a binary response. Predictive power is the area under the ROC curve.

Anatomical Analysis. Reanalysis of anatomical data (28, 29, 31) to estimate the relative positions of NEAR and FAR cell pairs is described in *Supporting Information* and Fig. S8.

ACKNOWLEDGMENTS. We thank Matthew Smith for constructive suggestions on the manuscript and Shin Nagayama and Takeshi Imai for sharing data. This work was funded by National Institutes of Health Awards DC010535, DC0005798, and DC0011184.

1. Kay LM, Sherman SM (2007) An argument for an olfactory thalamus. *Trends Neurosci* 30(2):47–53.
2. Johnson BA, Leon M (2007) Chemotopic odorant coding in a mammalian olfactory system. *J Comp Neurol* 503(1):1–34.
3. Harrison TA, Scott JW (1986) Olfactory bulb responses to odor stimulation: Analysis of response pattern and intensity relationships. *J Neurophysiol* 56(6):1571–1589.
4. Margrie TW, Schaefer AT (2003) Theta oscillation coupled spike latencies yield computational vigour in a mammalian sensory system. *J Physiol* 546(Pt 2):363–374.
5. Shusterman R, Smear MC, Koulakov AA, Rinberg D (2011) Precise olfactory responses tile the sniff cycle. *Nat Neurosci* 14(8):1039–1044.
6. Bathellier B, Buhl DL, Accolla R, Carleton A (2008) Dynamic ensemble odor coding in the mammalian olfactory bulb: Sensory information at different timescales. *Neuron* 57(4):586–598.
7. Cury KM, Uchida N (2010) Robust odor coding via inhalation-coupled transient activity in the mammalian olfactory bulb. *Neuron* 68(3):570–585.
8. Doucette W, et al. (2011) Associative cortex features in the first olfactory brain relay station. *Neuron* 69(6):1176–1187.
9. Stopfer M, Bhagavan S, Smith BH, Laurent G (1997) Impaired odour discrimination on desynchronization of odour-encoding neural assemblies. *Nature* 390(6655):70–74.
10. Nirenberg S, Latham PE (2003) Decoding neuronal spike trains: How important are correlations? *Proc Natl Acad Sci USA* 100(12):7348–7353.
11. Kashiwadani H, Sasaki YF, Uchida N, Mori K (1999) Synchronized oscillatory discharges of mitral/tufted cells with different molecular receptive ranges in the rabbit olfactory bulb. *J Neurophysiol* 82(4):1786–1792.
12. Dhawale AK, Hagiwara A, Bhalla US, Murthy VN, Albeanu DF (2010) Non-redundant odor coding by sister mitral cells revealed by light addressable glomeruli in the mouse. *Nat Neurosci* 13(11):1404–1412.
13. Averbeck BB, Latham PE, Pouget A (2006) Neural correlations, population coding and computation. *Nat Rev Neurosci* 7(5):358–366.
14. Cohen MR, Kohn A (2011) Measuring and interpreting neuronal correlations. *Nat Neurosci* 14(7):811–819.
15. Chen T-W, Lin B-J, Schild D (2009) Odor coding by modules of coherent mitral/tufted cells in the vertebrate olfactory bulb. *Proc Natl Acad Sci USA* 106(7):2401–2406.
16. Kazama H, Wilson RI (2009) Origins of correlated activity in an olfactory circuit. *Nat Neurosci* 12(9):1136–1144.
17. Zohary E, Shadlen MN, Newsome WT (1994) Correlated neuronal discharge rate and its implications for psychophysical performance. *Nature* 370(6485):140–143.
18. Ecker AS, Berens P, Tolias AS, Bethge M (2011) The effect of noise correlations in populations of diversely tuned neurons. *J Neurosci* 31(40):14272–14283.
19. Friedrich RW, Laurent G (2001) Dynamic optimization of odor representations by slow temporal patterning of mitral cell activity. *Science* 291(5505):889–894.
20. Cang J, Isaacson JS (2003) In vivo whole-cell recording of odor-evoked synaptic transmission in the rat olfactory bulb. *J Neurosci* 23(10):4108–4116.
21. Smith MA, Kohn A (2008) Spatial and temporal scales of neuronal correlation in primary visual cortex. *J Neurosci* 28(48):12591–12603.
22. de la Rocha J, Doiron B, Shea-Brown E, Josić K, Reyes A (2007) Correlation between neural spike trains increases with firing rate. *Nature* 448(7155):802–806.
23. Churchland MM, et al. (2010) Stimulus onset quenches neural variability: A widespread cortical phenomenon. *Nat Neurosci* 13(3):369–378.
24. Pillow JW, et al. (2008) Spatio-temporal correlations and visual signalling in a complete neuronal population. *Nature* 454(7207):995–999.
25. Truccolo W, Hochberg LR, Donoghue JP (2010) Collective dynamics in human and monkey sensorimotor cortex: Predicting single neuron spikes. *Nat Neurosci* 13(1):105–111.
26. Schneidman E, Berry MJ, 2nd, Segev R, Bialek W (2006) Weak pairwise correlations imply strongly correlated network states in a neural population. *Nature* 440(7087):1007–1012.
27. Buonviso N, Chaput MA, Scott JW (1991) Mitral cell-to-glomerulus connectivity: An HRP study of the orientation of mitral cell apical dendrites. *J Comp Neurol* 307(1):57–64.
28. Kikuta S, Fletcher ML, Homma R, Yamasoba T, Nagayama S (2013) Odorant response properties of individual neurons in an olfactory glomerular module. *Neuron* 77(6): 1122–1135.
29. Ke M-T, Fujimoto S, Imai T (2013) SeeDB: A simple and morphology-preserving optical clearing agent for neuronal circuit reconstruction. *Nat Neurosci* 16(8):1154–1161.
30. Egaña JI, Aylwin ML, Maldonado PE (2005) Odor response properties of neighboring mitral/tufted cells in the rat olfactory bulb. *Neuroscience* 134(3):1069–1080.
31. Buonviso N, Chaput MA, Berthommier F (1992) Temporal pattern analyses in pairs of neighboring mitral cells. *J Neurophysiol* 68(2):417–424.
32. Egger V, Urban NN (2006) Dynamic connectivity in the mitral cell-granule cell microcircuit. *Semin Cell Dev Biol* 17(4):424–432.
33. Kapoor V, Urban NN (2006) Glomerulus-specific, long-latency activity in the olfactory bulb granule cell network. *J Neurosci* 26(45):11709–11719.
34. Giridhar S, Doiron B, Urban NN (2011) Timescale-dependent shaping of correlation by olfactory bulb lateral inhibition. *Proc Natl Acad Sci USA* 108(14):5843–5848.
35. Ohiorhenuan IE, et al. (2010) Sparse coding and high-order correlations in fine-scale cortical networks. *Nature* 466(7306):617–621.
36. Ecker AS, et al. (2010) Decorrelated neuronal firing in cortical microcircuits. *Science* 327(5965):584–587.
37. Renart A, et al. (2010) The asynchronous state in cortical circuits. *Science* 327(5965): 587–590.
38. Bair W, Zohary E, Newsome WT (2001) Correlated firing in macaque visual area MT: Time scales and relationship to behavior. *J Neurosci* 21(5):1676–1697.
39. Miura K, Mainen ZF, Uchida N (2012) Odor representations in olfactory cortex: distributed rate coding and decorrelated population activity. *Neuron* 74(6):1087–1098.
40. Davison IG, Katz LC (2007) Sparse and selective odor coding by mitral/tufted neurons in the main olfactory bulb. *J Neurosci* 27(8):2091–2101.
41. Vincis R, Gschwend O, Bhaukaurally K, Beroud J, Carleton A (2012) Dense representation of natural odorants in the mouse olfactory bulb. *Nat Neurosci* 15(4):537–539.
42. Rinberg D, Koulakov A, Gelperin A (2006) Sparse odor coding in awake behaving mice. *J Neurosci* 26(34):8857–8865.
43. Blauvelt DG, Sato TF, Wienisch M, Knöpfel T, Murthy VN (2013) Distinct spatiotemporal activity in principal neurons of the mouse olfactory bulb in anesthetized and awake states. *Front Neural Circuits* 7:46.
44. Arevian AC, Kapoor V, Urban NN (2008) Activity-dependent gating of lateral inhibition in the mouse olfactory bulb. *Nat Neurosci* 11(1):80–87.
45. Cohen MR, Newsome WT (2008) Context-dependent changes in functional circuitry in visual area MT. *Neuron* 60(1):162–173.
46. Royet JP, Distel H, Hudson R, Gervais R (1998) A re-estimation of the number of glomeruli and mitral cells in the olfactory bulb of rabbit. *Brain Res* 788(1-2):35–42.
47. Padmanabhan K, Urban NN (2010) Intrinsic biophysical diversity decorrelates neuronal firing while increasing information content. *Nat Neurosci* 13(10):1276–1282.
48. Schmitzer-Torbert N, Jackson J, Henze D, Harris K, Redish AD (2005) Quantitative measures of cluster quality for use in extracellular recordings. *Neuroscience* 131(1):1–11.
49. Ventura V, Gerkin RC (2012) Accurately estimating neuronal correlation requires a new spike-sorting paradigm. *Proc Natl Acad Sci USA* 109(19):7230–7235.
50. Bozza T, Feinstein P, Zheng C, Mombaerts P (2002) Odorant receptor expression defines functional units in the mouse olfactory system. *J Neurosci* 22(8):3033–3043.
51. Benjamini Y, Hochberg Y (2009) Controlling the false discovery rate: A practical and powerful approach to multiple testing. *JR Stat Soc* 57:1.